# Spin-Current to Charge-Current Conversion and Magnetoresistance in a Hybrid Structure of Graphene and Yttrium Iron Garnet

J. B. S. Mendes,[1,*] O. Alves Santos,[2] L. M. Meireles,[3] R. G. Lacerda,[3] L. H. Vilela-Leão,[4] F. L. A. Machado,[2] R. L. Rodríguez-Suárez,[2,5] A. Azevedo,[2] and S. M. Rezende[2]

[1]*Departamento de Física, Universidade Federal de Viçosa, 36570-900 Viçosa, Minas Gerais, Brasil*
[2]*Departamento de Física, Universidade Federal de Pernambuco, 50670-901 Recife, Pernambuco, Brasil*
[3]*Departamento de Física, Universidade Federal de Minas Gerais, 31270-901 Belo Horizonte, Minas Gerais, Brasil*
[4]*Núcleo Interdisciplinar de Ciências Exatas e Inovação Tecnológica, Universidade Federal de Pernambuco, 55002-970 Caruaru, Pernambuco, Brasil*
[5]*Facultad de Física, Pontificia Universidad Católica de Chile, Casilla 306, Santiago, Chile*

(Received 25 May 2015; published 25 November 2015)

The use of graphene in spintronic devices depends, among other things, on its ability to convert a spin excitation into an electric charge signal, a phenomenon that requires a spin-orbit coupling (SOC). Here we report the observation of two effects that show the existence of SOC in large-area CVD grown single-layer graphene deposited on a single crystal film of the ferrimagnetic insulator yttrium iron garnet (YIG). The first is a magnetoresistance of graphene induced by the magnetic proximity effect with YIG. The second is the detection of a dc voltage along the graphene layer resulting from the conversion of the spin current generated by spin pumping from microwave driven ferromagnetic resonance into a charge current, which is attributed to the inverse Rashba-Edelstein effect.

DOI: 10.1103/PhysRevLett.115.226601 PACS numbers: 72.25.Mk, 75.70.Ak, 75.70.Cn, 76.50.+g

One key phenomenon for spintronics is the conversion of signals carried by spin excitations in ferromagnets (FM) into electric signals. In bilayers of FM with metallic layers (ML) this conversion involves the spin-pumping effect (SPE) [1,2] and the inverse spin Hall effect (ISHE) [3,4]. Precessing spins in the FM inject a spin current in the ML by the SPE, which is then converted into a charge current by the ISHE. This phenomenon was first observed by the electric detection of microwave driven ferromagnetic resonance (FMR) in multilayers of permalloy (Py), FeCo, and paramagnetic metals (PM) such as Pt, Pd, and Ta [5]. As the ISHE requires the presence of spin-orbit coupling (SOC), most SPE-ISHE studies have been conducted with PM materials of heavy elements [6]. Initially concentrated in bilayers with FM metals [3–8], the SPE-ISHE studies gained renewed interest with the discovery of spin pumping by the ferrimagnetic insulator yttrium iron garnet (YIG) [9–19]. The recent discovery [20,21] of new mechanisms for spin-current to charge-current conversion based on the Rashba-Edelstein effect has enriched the field and opened up new possibilities.

Owing to its exceptional electronic transport properties [22,23], graphene has been considered to be very promising for spintronic applications [24,25]. However, due to the low atomic number of carbon, intrinsic graphene has a weak SOC and thus very small spin Hall effect [26]. Several mechanisms and structures have been proposed for the use of graphene in spintronics, such as nanostructures with adjacent graphene nanoribbons [27], nanostructures with ferromagnetic gate electrodes [28,29], and decoration of graphene with small doses of adatoms or nanoparticles [30]. Recently, it has been shown that a Py electrode under FMR pumps spin current into a single-layer graphene (SLG) [31,32] and that SLG grown by chemical vapor deposition (CVD) on Cu foil carries Cu adatoms when transferred to a Si/SiO2 substrate and exhibits large SOC and spin-Hall effect [33].

Because of its very low magnetic damping, YIG is an ideal FM material to use in hybrid structures with graphene for spintronic applications. YIG has been the reference material for investigating a variety of magnonic phenomena [34,35]. The combination of the cm long magnon propagation length of YIG with the high carrier mobility of graphene might lead to spintronic devices with new functionalities. It has been shown theoretically that when a SLG is in atomic contact with a ferromagnetic insulator (FMI), there is a hybridization between the $\pi$ carbon orbitals in graphene and the neighboring spin-polarized $d$ orbitals in the FMI [36]. This gives rise to a proximity effect that results in long-range ferromagnetic ordering in graphene, as observed in YIG/SLG [37]. The interface exchange interaction is also required for the spin pumping from a FMI into a conducting layer [9,38]. In this Letter we report the observation of spin-current to charge-current conversion and magnetoresistance in large area CVD grown SLG on a YIG film. Both effects demonstrate that the SLG in atomic contact with YIG exhibits an extrinsic SOC that enhances the Rashba effect.

We have used a single-crystal YIG film with thickness 6.0 $\mu$m grown by liquid-phase epitaxy on a 0.5 mm thick

 © 2015 American Physical Society

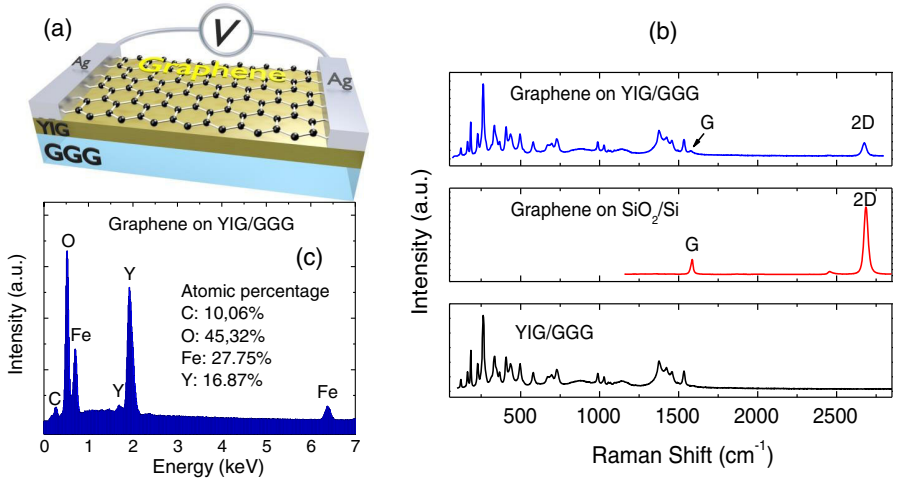


FIG. 1 (color online). (a) Illustration of the YIG/graphene structures and the electrodes used to measure the magnetoresistance and the dc voltage due to spin-current to charge-current conversion. At mm size scale, the graphene should be represented as a continuous layer. (b) Raman spectroscopy spectra of GGG/YIG, $SiO_2$/graphene, and GGG/YIG/graphene. (c) EDX spectrum from an arbitrary region in the sample of GGG/YIG/graphene.

substrate of (111) gallium gadolinium garnet (GGG). All samples were cut from the same GGG/YIG wafer in rectangular shape $1.5 \times 3.0$ mm$^2$, with the long dimension in a $\langle 111 \rangle$ axis. A SLG prepared on a copper foil, as described in Refs. [39,40] is transferred onto the YIG film and the sample receives two silver paint contacts as illustrated in Fig. 1(a). Figure 1(b) shows Raman spectroscopy spectra of GGG/YIG, $SiO_2$/SLG, and GGG/YIG/SLG. The spectrum at the top of the Fig. 1(b) shows the lines of GGG/YIG and the characteristic peaks $G$ (1580 cm$^{-1}$) and $2D$ (2700 cm$^{-1}$) bands of single-layer graphene, indicating successful transfer to YIG. The EDX spectrum of GGG/YIG/SLG in Fig. 1(c) shows the presence of Y, Fe, O, and C. The Cu adatoms from the copper foil which might be present have very low concentrations since they are not visible in the EDX spectrum [41].

Both the magnetoresistance and spin-current to charge-current conversion were investigated at room temperature with the YIG/SLG structure illustrated in Fig. 1(a). The change $\Delta R$ in the resistance $R$ between the two electrodes was measured with varying magnetic field applied in the plane perpendicularly to the long sample dimension. Since graphene is nonmagnetic and YIG is insulating, all changes in the transport properties with field are attributed to the proximity effect, similarly to the effect in YIG/Pt [42]. In order to correlate the magnetoresistance with the magnetization of YIG, we show in the inset of Fig. 2(a) the measured magnetization of the YIG/SLG sample as a function of the magnetic field in the same direction used to measure the resistance. The data show a small hysteresis, with a coercive field 1.8 Oe and remanent magnetization 0.12 of the saturation value. The linear current versus voltage ($I$-$V$) curve measured between the electrodes, shown in the inset of Fig. 2(b), demonstrates the formation of Ohmic contacts between the electrodes and SLG. From the measured $I$-$V$ curve the resistance of the SLG between the electrodes is 3.4 kΩ, consistent with values obtained for CVD graphene grown on Cu foils [43].

Since the absolute variation of the resistance $R$ with magnetic field $H$ is quite small, to obtain reliable data on the magnetoresistance we have employed a modulation technique and lock-in amplifier detection. A constant current of 0.3 mA is injected in the YIG/SLG device while the magnetic field is modulated with amplitude 4 Oe and frequency 26 kHz. The voltage measured in the lock-in amplifier represents the change in resistance with field, as shown in Fig. 2(b). The results with increasing and decreasing field exhibit two nearly identical peaks with small hysteresis. The data in Fig. 2(b) can be explained with Kohler's rule for the magnetoresistance, $\mathrm{MR} = \Delta R/R \propto (M_G)^2$, where $M_G$ is the SLG magnetization created by the long-range order induced by the proximity effect [36,37]. Since $M_G$ is proportional to the YIG magnetization $M$, with ac field modulation the change in resistance is $\mathrm{MR} \propto (M + \Delta M)^2 \approx M^2 + 2M\,\Delta M$, where $\Delta M$ is determined by the amplitude of the field modulation $\delta H$. Hence, the ac component of the magnetoresistance is $\Delta\mathrm{MR} \propto |M(dM/dH)|\delta H$. Figure 2(a) shows $|M(dM/dH)|$ calculated from the $M$ vs $H$ data points. The excellent agreement between the positions of the peaks in the measured MR and the calculated ones is an evidence of two effects of the proximity induced magnetism of graphene on YIG: (i) There is an interface exchange interaction between the

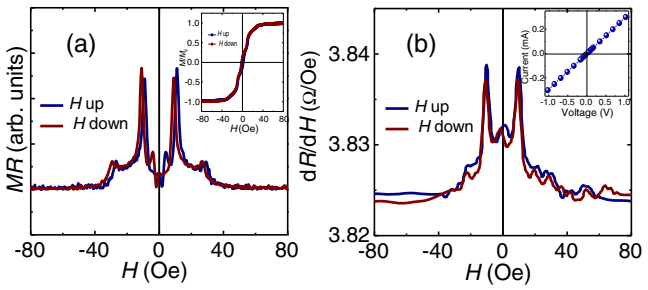


FIG. 2 (color online). (a) Magnetoresistance versus field $H$ calculated from the $M$ vs $H$ data of YIG/SLG (shown in the inset), as a function of the field applied in plane, transverse to the long dimension. (b) Measured field derivative of the resistance of graphene on YIG with increasing and decreasing field. Inset shows the $I$-$V$ curve of the YIG/SLG structure demonstrating the formation of Ohmic contacts between the electrodes and the SLG.

spins in YIG and the spins of the carriers in SLG, manifested by the relation $M_G \propto M$; (ii) graphene on YIG exhibits spin-orbit coupling, since this is necessary for the change in resistance with magnetic field.

In the spin-current to charge-current conversion experiments, the FM/ML bilayer sample is subjected to a microwave magnetic field perpendicular to the static field in the FMR configuration. The precessing magnetization $\vec{M}$ in the FM layer generates a spin current at the FM/ML interface with density $\vec{J}_S = (\hbar g_{\rm eff}^{\uparrow\downarrow}/4\pi M^2)(\vec{M} \times \partial\vec{M}/\partial t)$, where $g_{\rm eff}^{\uparrow\downarrow}$ is the real part of the interface spin mixing conductance, that takes into account the spin-pumped and backflow spin currents [1,2]. The spin current that flows into the adjacent conducting layer produces two effects: (i) Increased damping of the magnetic excitation due to the out-flow of spin angular momentum [1,2,6–8]; (ii) conversion into a charge current that produces a voltage at the ends of the metallic layer.

In order to compare the data on the spin-current to charge-current conversion in YIG/SLG with a well studied system, we have also measured the spin-pumping voltage in a sample made from the same GGG/YIG (6 $\mu$m) wafer, with dimensions $1.5 \times 3.0$ mm$^2$, capped with a 4 nm thick Pt layer, deposited by dc magnetron sputtering. For the FMR microwave absorption and spin-current to charge-current conversion measurements, the sample with electrodes as in Fig. 1(a), is mounted on the tip of a PVC rod and inserted into a small hole in the back wall of a shorted waveguide setup, in a position of maximum rf magnetic field and zero electric field. The waveguide is placed between the poles of an electromagnet so that the sample can be rotated while maintaining the static and rf fields in the plane and perpendicular to each other. With this configuration we can investigate the angular dependence of the spectra. Field scan spectra of the derivative $dP/dH$ of the microwave absorption are obtained by modulating the field at 1.2 kHz and using lock-in detection. Figure 3 shows the FMR spectra of three samples, all obtained with $H$ in plane and normal to the long strip dimension, frequency $f = 9.4$ GHz, and input microwave power 32 mW. In Fig. 3(a) for a bare YIG film one clearly sees the various lines corresponding to standing spin-wave modes with quantized wave numbers $k$ due to the boundary conditions at the edges of the film. The strongest line corresponds to the uniform (FMR) mode that has frequency close to the spin-wave mode with $k = 0$, given by $\omega_0 \approx \gamma H^{1/2}(H+4\pi M)^{1/2}$, where $\gamma = 2\pi \times 2.8$ GHz/kOe for YIG and $4\pi M$ is the saturation magnetization (1.76 kG at room temperature). The lines to the left of the FMR correspond to hybridized standing spin-wave surface modes whereas those to the right are volume modes. All modes have similar peak-to-peak linewidth of 0.36 Oe, corresponding to a half-width-at-half-maximum (HWHM) of $\Delta H_{\rm FM} \approx 0.31$ Oe.

The contact of the YIG film with the metallic layer produces two effects on the microwave absorption spectra. As can be seen in Figs. 3(b) and 3(c), all spectra shift uniformly to lower fields, indicating that the metallic layer creates a surface anisotropy field [11]. The other effect is the line broadening caused by the fact that the spin current created by spin pumping carries angular momentum out of the FMI layer. From the spectra in Fig. 3 we obtain the values of the HWHM for YIG/Pt and YIG/SLG, respectively, 0.91 and 0.54 Oe, both larger than 0.31 Oe for bare YIG. In the case of the YIG/Pt sample, from the measured linewidths with and without the metallic layer, $\Delta H_{\rm FM/ML}$ and $\Delta H_{\rm FM}$, one can obtain the real part of the effective interface spin mixing conductance. It is given by $g_{\rm eff}^{\uparrow\downarrow} = (4\pi M\, t_{\rm FM}/\hbar\omega)\,(\Delta H_{\rm FM/ML} - \Delta H_{\rm FM})$, where $\omega = 2\pi f$ and $t_{\rm FM}$ is the FM film thickness for very thin YIG films or a coherence length for thick films such as the one used here [14–16,38,44–46]. As pointed out in Ref. [32], for a FMI/SLG bilayer, one expects a similar expression to hold, as long as the spin current pumped into the SLG relaxes much faster than the charge diffuses. We assume that this is the case here, so that from the measured value of $g_{\rm eff}^{\uparrow\downarrow}$ for YIG/Pt we can infer the value for YIG/SLG considering that its linewidth change relative to that in YIG/Pt is 0.38.

The spin-current to charge-current conversion experiments were done with the samples used in the FMR measurements, as sketched in the inset of Fig. 4(a). The wires were connected to a nanovoltmeter for a direct measurement of the spin-pumping voltage $V_{\rm SP}(H)$ spectrum obtained with $H$ field sweep and no ac field modulation. By rotating the sample in the plane we measure the dependence of the voltage on the angle $\phi$. Figure 4 shows the spectra of $V_{\rm SP}(H)$ obtained with microwave frequency $f = 9.4$ GHz and incident power of 150 mW, with $H$ at $\phi = 0°$, 90°, 180°. Figure 4(a) shows the spectrum for YIG/Pt, with a large peak of about 10 $\mu$V at the FMR field position and lateral small peaks corresponding to the standing spin-wave modes. The voltage peaks change sign

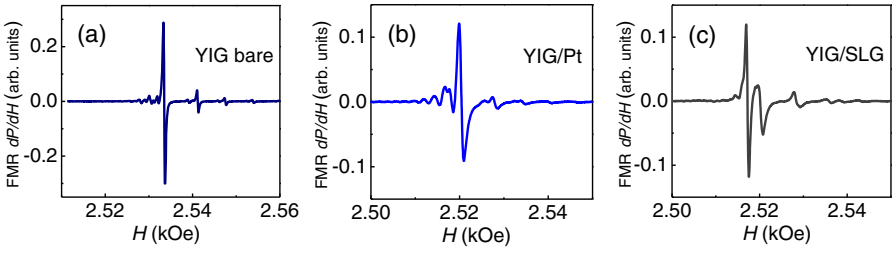


FIG. 3 (color online). Field scan FMR microwave absorption derivative spectra at a frequency 9.4 GHz of three samples of 6 $\mu$m thick YIG film capped as indicated, with lateral dimensions $1.5 \times 3.0$ mm$^2$, with the magnetic field applied in the film plane, normal to the long dimension.

when the sample is rotated by 180° and fall to noise level when $\phi = 90°$. Figure 4(b) shows that the voltage measured in the YIG/SLG sample exhibits spin-pumping voltage with features similar to other metals. However, there is an asymmetry between the positive and negative peaks, which is similar to that observed in YIG/Py [17]. This is another indication of the ferromagnetic order in the graphene layer due to the proximity effect of YIG. The inset in Fig. 4(b) shows that the peak voltage in YIG/SLG increases linearly with the microwave power showing that nonlinear effects are not present in the power range of the experiments.

The dc spin-pumping spin-current density at the YIG/ML interface generated by the magnetization precession is [8]

$$J_S(0) = \frac{\hbar\omega p g_{\rm eff}^{\uparrow\downarrow}}{4\pi}\left(\frac{h}{\Delta H}\right)^2 L(H - H_R), \qquad (1)$$

where $\Delta H$ and $H_R$ are, respectively, the linewidth and field for resonance of the YIG/ML bilayer, $L(H - H_R)$ is the Lorentzian line shape and $p$ is the precession ellipticity. In all studies reported to date for FMI/ML bilayers, the mechanism for conversion of the spin current in Eq. (1) into a charge current is the inverse spin Hall effect [4–18]. Recently, Rojas Sánchez [20] showed that in a multilayer system, a spin current can be converted into a charge current by the inverse Rashba-Edelstein effect (IREE) at the interface between two nonmagnetic layers. In the case of the YIG/Pt bilayer, the spin current flows into the Pt layer and diffuses, with a spin diffusion length $\lambda_N$. Then it is converted into a charge current with density $\vec{J}_C = \theta_{\rm SH}(e/\hbar)\vec{J}_S \times \vec{\sigma}$ by means of the ISHE, where $\theta_{\rm SH}$ is the spin Hall angle and $\vec{\sigma}$ the spin polarization defined by the applied field. Integration of the current density leads to the dc voltage [6–8]

$$V_{\rm SP}(H) = R_N \frac{\omega\, e\theta_{\rm SH}\lambda_N w\, p_{xz}\, g_{\rm eff}^{\uparrow\downarrow}}{8\pi} \times \tanh(t_N/2\lambda_N)\left(\frac{h}{\Delta H}\right)^2 L(H - H_R)\cos\phi, \qquad (2)$$

where $R_N$, $t_N$, and $w$ are, respectively, the resistance, thickness and width of the Pt layer, and $p_{xz}$ is a factor that expresses the ellipticity and the spatial variation of the rf magnetization of the FMR mode. We use for Pt (4 nm) the measured resistance $R_N = 178\ \Omega$ and the parameters $\theta_{\rm SH} = 0.08$, $\lambda_N = 3.7$ nm [8], and for YIG $p_{1,1} = 0.31$ appropriate for the uniform (1,1) mode at 9.4 GHz [18], and FMR linewidth $\Delta H = 0.91$ Oe. Using $h = 4.8 \times 10^{-2}$ Oe, corresponding to a microwave power of 150 mW in the shorted waveguide, and the peak value $V_{\rm SP} = 10\ \mu$V in Fig. 4(a), we find with Eq. (2) that $g_{\rm eff}^{\uparrow\downarrow} \approx 10^{18}$ m$^{-2}$, consistent with values for YIG/Pt in the literature [6,16,45].

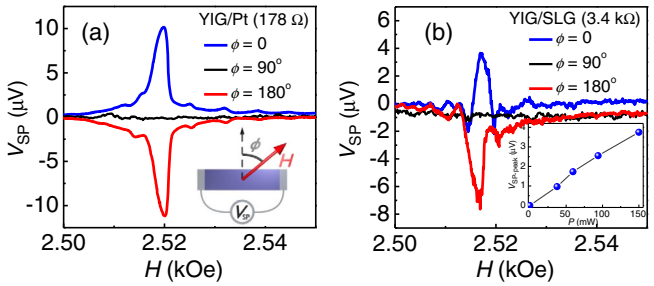


FIG. 4 (color online). Field scan spin-pumping dc voltage measured with 9.4 GHz microwave driving with power 150 mW in YIG(6 $\mu$m)/Pt(4 nm) and YIG(6 $\mu$m)/SLG, with the magnetic field applied in the film plane at the angles indicated in the inset of (a). The inset in (b) shows the linear variation of the peak voltage with microwave power in YIG/SLG.

One might attempt to interpret the origin of the voltage in YIG/SLG with the same spin-pumping ISHE mechanism, as done in Ref. [47]. To apply Eq. (2) for YIG/SLG we consider $t_N/2\lambda_N \ll 1$, so that $V_{\rm SP} = (R_N f e\theta_{\rm SH} w p_{xz} g_{\rm eff}^{\uparrow\downarrow} t_N/8)(h/\Delta H)^2$. This expression does not depend on the spin diffusion length, as expected for a single atomic layer, but it requires that an effective thickness $t_N$ is attributed SLG. With $R_N = 3400\ \Omega$, $g_{\rm eff}^{\uparrow\downarrow} \approx 4 \times 10^{17}$ m$^{-2}$ obtained from the FMR linewidth increase in YIG/SLG, $\theta_{\rm SH} = 0.2$ reported in Ref. [33] for CVD graphene grown on Cu foil, the SLG thickness that would give the measured voltage in Fig. 4(b), $V_{\rm SP} = 5\ \mu$V, is $t_N = 2 \times 10^{-11}$ m. This is too small compared to any effective thickness ascribed to a single-layer graphene [48], which is certainly nonphysical. Thus, the spin-pumping voltage observed in YIG/SLG cannot be attributed to the SPE ISHE effect, which is not unexpected since in SLG the spin-pumping spin-current cannot have a 3D component.

We follow Ref. [20] and interpret the spin-current to charge-current conversion in SLG as arising from the inverse Rashba-Edelstein effect, made possible by the extrinsic SOC due mainly to the proximity effect with YIG. The 3D spin current in Eq. (1) flows into the SLG and is converted by the IREE into a charge current in the single layer graphene with a 2D density $j_C = (2e/\hbar)\lambda_{\rm IREE} J_S$, where $\lambda_{\rm IREE}$ is a coefficient characterizing the IREE, with dimension of length and proportional to the Rashba coefficient, and hence to the magnitude of the SOC [49]. The measured voltage is related to this current density by $V_{\rm IREE} = R_N w j_C$. Using the same parameters as before, we find for the IREE coefficient $\lambda_{\rm IREE} \approx 10^{-3}$ nm. This value is about 2 orders of magnitude smaller than the one obtained in Ref. [20] for the Ag/Bi interface. This is not surprising, since Bi is known to have a large SOC, whereas in SLG the SOC arises from extrinsic sources and is certainly smaller.

In summary, we have observed two effects in large-area CVD grown single-layer graphene deposited on a single crystal film of yttrium iron garnet that show the existence of SOC. The first is a magnetoresistance of graphene induced by the magnetic proximity effect with YIG. The second is the detection of a dc voltage along the graphene layer resulting from the conversion of the spin current generated by spin pumping from microwave driven FMR into charge current. We interpret the spin-current to charge-current conversion as arising from the inverse Rashba-Edelstein

effect made possible by the extrinsic spin-orbit coupling in graphene. These observations show that spin-orbit coupling can be extrinsically enhanced in graphene by the proximity effect with a ferromagnetic layer.

The authors would like to thank Professor Alexandre R. Rodrigues for the measurement of the YIG magnetization, Professor Luciano G. Moura for assistance in the Raman measurements, José Holanda, Pablo T. Ribeiro, and Juan M. Marín for assistance in the magnetoresistance measurements. Research supported in Brazil by the agencies CNPq, CAPES, FINEP, FAPEMIG, FACEPE, INCT de Nanocarbono, and Rede de Nanoinstrumentação, and in Chile by FONDECYT No. 1130705.

*Corresponding author.
joaquim.mendes@ufv.br

[1] Y. Tserkovnyak, A. Brataas, and G. E. W. Bauer, Phys. Rev. Lett. **88**, 117601 (2002).
[2] Y. Tserkovnyak, A. Brataas, G. E. W. Bauer, and B. I. Halperin, Rev. Mod. Phys. **77**, 1375 (2005).
[3] J. E. Hirsch, Phys. Rev. Lett. **83**, 1834 (1999).
[4] E. Saitoh, H. Miyajima, and G. Tatara, Appl. Phys. Lett. **88**, 182509 (2006).
[5] A. Azevedo, L. H. Vilela Leão, R. L. Rodriguez-Suarez, A. B. Oliveira, and S. M. Rezende, J. Appl. Phys. **97**, 10C715 (2005).
[6] A. Hoffmann, IEEE Trans. Magn. **49**, 5172 (2013).
[7] O. Mosendz, V. Vlaminck, J. E. Pearson, F. Y. Fradin, G. E. W. Bauer, S. D. Bader, and A. Hoffmann, Phys. Rev. B **82**, 214403 (2010).
[8] A. Azevedo, L. H. Vilela-Leão, R. L. Rodríguez-Suárez, A. F. Lacerda Santos, and S. M. Rezende, Phys. Rev. B **83**, 144402 (2011).
[9] Y. Kajiwara *et al.*, Nature (London) **464**, 262 (2010).
[10] C. W. Sandweg, Y. Kajiwara, K. Ando, E. Saitoh, and B. Hillebrands, Appl. Phys. Lett. **97**, 252504 (2010).
[11] L. H. Vilela-Leão, C. Salvador, A. Azevedo, and S. M. Rezende, Appl. Phys. Lett. **99**, 102505 (2011).
[12] K. Ando, T. Na, and E. Saitoh, Appl. Phys. Lett. **99**, 092510 (2011).
[13] C. Hahn, G. de Loubens, O. Klein, M. Viret, V. V. Naletov, and J. Ben Youssef, Phys. Rev. B **87**, 174417 (2013).
[14] *Recent Advances in Magnetic Insulators-From Spintronics to Microwave Applications, Solid State Physics*, edited by M. Wu and A. Hoffmann (Academic Press, Burlington, 2013), Vol. 64.
[15] M. B. Jungfleisch, A. V. Chumak, A. Kehlberger, V. Lauer, D. H. Kim, M. C. Onbasli, C. A. Ross, M. Kläui, and B. Hillebrands, Phys. Rev. B **91**, 134407 (2015).
[16] C. Du, H. Wang, P. Chris Hammel, and F. Yang, J. Appl. Phys. **117**, 172603 (2015).
[17] A. Azevedo, O. Alves Santos, G. A. Fonseca Guerra, R. O. Cunha, R. Rodríguez-Suárez, and S. M. Rezende, Appl. Phys. Lett. **104**, 052402 (2014).
[18] J. B. S. Mendes *et al.*, Phys. Rev. B **89**, 140406(R) (2014).
[19] W. Zhang, M. B. Jungfleisch, W. Jiang, J. E. Pearson, A. Hoffmann, F. Freimuth, and Y. Mokrousov, Phys. Rev. Lett. **113**, 196602 (2014).
[20] J. C. Rojas Sánchez *et al.*, Nat. Commun. **4**, 2944 (2013).
[21] C. Ciccarelli, K. M. D. Hals, A. Irvine, V. Novak, Y. Tserkovnyak, H. Kurebayashi, A. Brataas, and A. Ferguson, Nat. Nanotechnol. **10**, 50 (2014).
[22] K. S. Novoselov *et al.*, Science **306**, 666 (2004).
[23] A. H. Castro Neto, F. Guinea, N. M. R. Peres, K. S. Novoselov, and A. K. Geim, Rev. Mod. Phys. **81**, 109 (2009).
[24] D. Pesin and A. H. MacDonald, Nat. Mater. **11**, 409 (2012).
[25] N. Tombros, C. Jozsa, M. Popinciuc, H. T. Jonkman, and B. J. van Wees, Nature (London) **448**, 571 (2007).
[26] D. Huertas-Hernando, F. Guinea, and A. Brataas, Phys. Rev. B **74**, 155426 (2006).
[27] S.-H. Chen, B. K. Nikolic, and C.-R. Chang, Phys. Rev. B **81**, 035428 (2010).
[28] Q. Zhang, Z. Lin, and K. S. Chan, J. Phys. Condens. Matter **24**, 075302 (2012).
[29] D. Bercioux, D. F. Urban, F. Romeo, and R. Citro, Appl. Phys. Lett. **101**, 122405 (2012).
[30] A. Ferreira, T. G. Rappoport, M. A. Cazalilla, and A. H. Castro Neto, Phys. Rev. Lett. **112**, 066601 (2014).
[31] Z. Tang *et al.*, Phys. Rev. B **87**, 140401(R) (2013).
[32] S. Singh, A. Ahmadi, C. T. Cherian, E. R. Mucciolo, E. del Barco, and B. Özyilmaz, Appl. Phys. Lett. **106**, 032411 (2015).
[33] J. Balakrishnan *et al.*, Nat. Commun. **5**, 4748 (2014).
[34] A. A. Serga, A. V. Chumak, and B. Hillebrands, J. Phys. D **43**, 264002 (2010).
[35] S. M. Rezende, F. M. de Aguiar, and O. F. de Alcantara Bonfim, J. Magn. Magn. Mater. **54–57**, 1127 (1986); S. M. Rezende and F. M. de Aguiar, Proc. IEEE **78**, 893 (1990).
[36] H. X. Yang, A. Hallal, D. Terrade, X. Waintal, S. Roche, and M. Chshiev, Phys. Rev. Lett. **110**, 046603 (2013).
[37] Z. Wang, C. Tang, R. Sachs, Y. Barlas, and J. Shi, Phys. Rev. Lett. **114**, 016603 (2015).
[38] S. M. Rezende, R. L. Rodríguez-Suárez, and A. Azevedo, Phys. Rev. B **88**, 014404 (2013).
[39] I. Silvestre, A. W. Barnard, S. P. Roberts, P. L. McEuen, and R. G. Lacerda, Appl. Phys. Lett. **106**, 153105 (2015).
[40] I. D. Barcelos, L. G. Moura, R. G. Lacerda, and A. Malachias, Nano Lett. **14**, 3919 (2014).
[41] See the Supplemental Material at http://link.aps.org/supplemental/10.1103/PhysRevLett.115.226601 for more details about the conditions of growth and transferring of graphene, the sample preparation, the crystallographic structure of the YIG, and additional data analysis involving the results EDX measurements.
[42] S. Y. Huang, X. Fan, D. Qu, Y. P. Chen, W. G. Wang, J. Wu, T. Y. Chen, J. Q. Xiao, and C. L. Chien, Phys. Rev. Lett. **109**, 107204 (2012).
[43] A. Avsar *et al.*, Nat. Commun. **5**, 4875 (2014).
[44] B. Heinrich, C. Burrowes, E. Montoya, B. Kardasz, E. Girt, Y.-Y. Song, Y. Sun, and M. Wu, Phys. Rev. Lett. **107**, 066604 (2011).
[45] M. Weiler *et al.*, Phys. Rev. Lett. **111**, 176601 (2013).
[46] S. M. Rezende, R. L. Rodríguez-Suárez, M. M. Soares, L. H. Vilela-Leão, D. Ley Domínguez, and A. Azevedo, Appl. Phys. Lett. **102**, 012402 (2013).
[47] R. Ohshima, A. Sakai, Y. Ando, T. Shinjo, K. Kawahara, H. Ago, and M. Shiraishi, Appl. Phys. Lett. **105**, 162410 (2014).
[48] Z. H. Ni, H. M. Wang, J. Kasim, H. M. Fan, T. Yu, Y. H. Wu, Y. P. Feng, and Z. X. Shen, Nano Lett. **7**, 2758 (2007).
[49] K. Shen, G. Vignale, and R. Raimondi, Phys. Rev. Lett. **112**, 096601 (2014).